PAPER • OPEN ACCESS

Nonequilibrium depinning transition of ac driven vortices with random pinning

To cite this article: Y Kawamura *et al* 2017 *New J. Phys.* **19** 093001

New Journal of Physics
The open access journal at the forefront of physics

Deutsche Physikalische Gesellschaft DPG
IOP Institute of Physics

Published in partnership with: Deutsche Physikalische Gesellschaft and the Institute of Physics

OPEN ACCESS

RECEIVED
15 May 2017

REVISED
19 July 2017

ACCEPTED FOR PUBLICATION
24 July 2017

PUBLISHED
5 September 2017

PAPER

Nonequilibrium depinning transition of ac driven vortices with random pinning

Y Kawamura[1], **S Moriya, K Ienaga, S Kaneko and S Okuma**

Department of Physics, Tokyo Institute of Technology, 2-12-1, Ohokayama, Meguro-ku, Tokyo 152–8551, Japan
[1] Present address: National Metrology Institute of Japan (NMIJ), AIST, 1-1-1, Umezono, Tsukuba, Ibaraki 305–8563, Japan.

E-mail: sokuma@o.cc.titech.ac.jp

Keywords: vortex pinning, deformation and plasticity, dynamic critical phenomena

Abstract

We study the critical behavior associated with transient dynamics of vortices near the depinning transition by an ac drive. From $I_{ac,e}$–$V_{ac,e}$ curves at different frequencies f, where $I_{ac,e}$ and $V_{ac,e}$ are the effective current and voltage of sinusoidal waveform, respectively, we clearly identify the characteristic voltage separating linear and nonlinear regimes, from which we can estimate the mean diameter of the pinning potential. We also measure the time evolution of the voltage $V_{ac}(t)$ for a disordered initial vortex configuration in response to the ac drive $I_{ac}(t)$ of square waveform, and find a gradual increase in the amplitude $|V_{ac}(t)|$ towards the steady-state voltage, indicative of dynamic ordering. The relaxation time $\tau(f)$ against $|I_{ac}(f)|$ shows a power-law divergence at the f-dependent depinning threshold $I_{ac,d}(f)$. When plotted against $|I_{ac}(f)| - I_{ac,d}(f)$, all $\tau(f)$'s collapse on a single line with a critical exponent of 1.4, which almost coincides with the value for the dc depinning transition. These results indicate that the critical behavior of the depinning transition is observed not only for the dc drive but also for the ac drive, further demonstrating the universality of the nonequilibrium depinning transition.

1. Introduction

Dynamic properties of driven elastic objects interacting with a random pinning substrate are determined by the competition between disorder of the substrate and the elasticity of the lattice [1–27]. As the pinning strength exceeds the elasticity, the lattice is deformed plastically. When a dc driving force F is applied abruptly, some particles constituting the lattices move in the form of fluctuating channels while others remain pinned [1, 2]. The transient dynamics is largely dependent on the initial configuration of the particles. For an ordered initial configuration where a small number of particles are pinned by random pinning centers or, equivalently, an ordered lattice involving a small number of dislocations (topological defects), the driven particles are gradually pinned to random pinning sites until the final steady ($t \to \infty$) state is reached. This process is called a dynamic disordering or dynamic pinning. When the applied dc force F is below a critical depinning force F_c, all the particles are pinned in the final steady state, while for $F > F_c$, a nonzero number of particles remain moving in the final state. Although the transient behavior associated with the dynamic disordering was observed in earlier experiments on the vortex dynamics of single crystal $NbSe_2$ [6], the existence of the nonequilibrium depinning transition was predicted in more recent numerical simulations. According to [2], it could be detected from the transient vortex dynamics associated with the dynamic disordering near F_c.

Recently, we have provided evidence of the nonequilibrium depinning transition [2] in a vortex system with a Corbino disk geometry for an amorphous (a-)Mo_xGe_{1-x} film with weak random pinning [18]. In the experiment, we first prepared an ordered initial vortex configuration with a small number of pinned vortices. Then, a dc current I with a sharp rise was applied to it at $t = 0$ and a time(t)-evolution of the voltage $V(t)$ generated by vortex motion was measured, where I and V correspond to the dc driving force F and the mean vortex velocity v, respectively. We observed a decay of $V(t)$ towards a final steady-state voltage $V(t \to \infty)(\equiv V^{\infty})$, indicative of the dynamic disordering (pinning). The relaxation time τ for the system to

settle into the steady state is dependent on I and exhibits a power-law divergence $\tau \propto (I - I_d)^{-\nu_{dc}}$ at around the depinning current I_d determined from the I–V characteristics [18]. The value of the critical exponent ν_{dc} is around 1.3–1.4, which is nearly equal to the value $\nu_{dc} = 1.3$–1.4 predicted theoretically [2]. Soon after, the similar diverging behavior of τ has been reported on both sides of the threshold current in the single crystal of NbS_2 [28], where the transition is caused by 'jamming' of vortices at high driving currents. The reported values of $\tau \sim 10^3$ s are significantly (by five orders of magnitude) larger than $\tau \sim 10^{-2}$ s in our a-Mo_xGe_{1-x} films, while the reported $\nu_{dc} \approx 1.6$ in the NbS_2 crystal is only slightly larger than $\nu_{dc} = 1.3$–1.4 in the a-Mo_xGe_{1-x} films.

We have extended our experiment to include a *disordered* initial vortex configuration, and found that $V(t)$ in response to the dc drive I shows a gradual *increase* and relaxation towards V^∞, indicative of the dynamic *ordering* (*depinning*) [29]. Nevertheless, the relaxation time exhibits a power-law divergence at the same current I_d and with the same exponent as those found for the ordered initial configuration. These results indicate that, while the transient behavior is largely dependent on the initial vortex configuration, the critical behaviors as well as the final mean velocity of vortices [25] are nearly identical to each other.

Previous experimental and numerical studies on the nonequilibrium depinning transition have focused only on the response to the dc drive, while it is well known for the vortex system that the ac external forces, namely, the ac current I_{ac} and the ac magnetic field, are readily used to depin and order the vortex lattice [9, 13, 24, 25, 30–33]. For the ac current–voltage ($|I_{ac}|$–$|V_{ac}|$) characteristics, an increase in the frequency f as well as the amplitude $|I_{ac}|$ of the ac drive I_{ac} causes an enhancement of the amplitude $|V_{ac}|$ of the ac voltage. Figure 1 of [24] shows the results of the numerical simulation, where the amplitude of the ac velocity is plotted against the amplitude of the ac driving force at different frequencies ω, including the dc case ($\omega = 0$). It is clearly seen that with an increase in ω, the velocity shows an increase. This is qualitatively explained in terms of reduced-pinning or reduced-dislocation effects by shaking the vortices at higher frequencies. Apart from the frequency-dependent effects, the determination of the depinning threshold for the ac driven vortices is more difficult than for the dc driven ones. This is because, even when the mean displacement of the vortex motion becomes smaller than the diameter of the pinning-potential well by decreasing the amplitude of the ac drive, and the vortices are 'trapped' in the potential well, the detectable voltage V_{ac} is generated due to the small harmonic oscillations persisting inside the pinning-potential well. The simulation of [24] reasonably predicted that the mean displacement of the lattice, rather than the mean velocity, is a relevant quantity in identifying depinning and dynamical ac regimes. To the best of our knowledge, however, this prediction has not been explicitly verified by experiment. Furthermore, if the depinning threshold is determined for the ac driven vortices, then it is of great interest to investigate whether the critical behavior of the nonequilibrium depinning transition is also observed for the ac drive. Again, this question has not yet been answered theoretically or experimentally.

In this work, we start with measurements of $|I_{ac}|$–$|V_{ac}|$ characteristics, where we use I_{ac} of sinusoidal waves with various frequencies f. All the data that we present in this paper were taken at 4.1 K in 2.0 T, corresponding to the ordered or weakly disordered vortex-lattice phase at equilibrium [37], where the pinning strength is moderate. We know from our previous work on the dc depinning transition [34] that the critical dynamics associated with dynamic disordering near the depinning transition is commonly observed in different vortex phases except in the disordered phase just prior to the liquid phase. In this work, by plotting the $I_{ac,e}$–$V_{ac,e}$ relation, where $I_{ac,e}$ and $V_{ac,e}$ denote the effective current and voltage, respectively, we clearly identify the f-dependent effective current $I_{ac,es}$ and voltage $V_{ac,es}$ separating the linear response regime ($V_{ac,e} < V_{ac,es}$) where the vortices oscillate inside the pinning-potential well from the nonlinear regime ($V_{ac,e} > V_{ac,es}$) where the vortices are depinned (escape) from the pinning potential. From the characteristic values of $V_{ac,es}(f)$, the mean diameter of the pinning potential is estimated. Next, to examine the critical behavior of the ac depinning transition associated with dynamic ordering, we perform transient measurements of $V_{ac}(t)$ for the disordered initial vortex configuration in response to $I_{ac}(t)$ of square waveform. $|V_{ac}(t)|$ shows a gradual increase and relaxation towards the steady-state value $|V_{ac}(t \to \infty)|(\equiv V^\infty)$, reflecting the dynamic ordering. The relaxation time τ for the system to reach the steady state increases with a decrease in $|I_{ac}|$, and exhibits a power-law divergence at around the f-dependent depinning threshold $I_{ac,d}$, similarly to what has been observed in the dc drive [18, 29, 34]. All the data of τ at different f plotted against $|I_{ac}| - I_{ac,d}$ fall onto nearly a single line, which gives a well-defined critical exponent $\nu = 1.4$ close to $\nu_{dc} = 1.3$–1.4 for the dc drive.

2. Experiment

A strip-shaped film of a-Mo_xGe_{1-x} with a thickness of 0.35 μm was prepared by rf sputtering on a silicon substrate mounted on a water cooled rotating copper stage [18, 34–37]. The mean-field transition temperature defined by a 95% criterion of the normal-state resistivity and zero-resistivity temperature are 6.85 and 6.71 K, respectively. The dc linear resistivity, and dc and ac current–voltage characteristics were measured using a

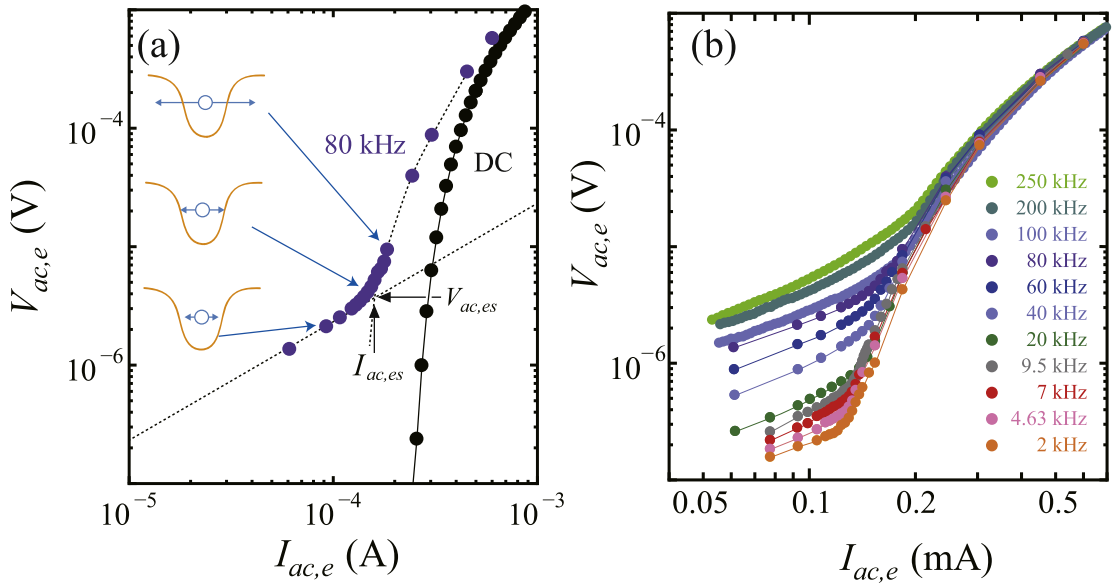

Figure 1. (a) $I_{ac,e}$–$V_{ac,e}$ characteristics (purple circles) for a sinusoidal current with $f = 80$ kHz and dc I–V characteristics (black circles). A straight dotted line represents a linear relation and other lines are guide for the eye. Inset: schematic diagram of the pinning-potential well and a vortex oscillating around the center of the well. (b) $I_{ac,e}$–$V_{ac,e}$ characteristics taken at various f listed in the figure. The lines are a guide for the eye.

standard four-terminal method. In the ac current–voltage measurements we applied ac currents of either sinusoidal or square waveform to the vortex system, and voltages induced by the vortex motion were measured using a lock-in amplifier or an ac digital voltmeter, respectively, after amplified with preamplifiers. We also measured the time evolution of voltage $V_{ac}(t)$ just after the ac current I_{ac} of square waveform was applied, whose amplitude was adjusted to yield an ac voltage with desired amplitude V^{∞} in the steady state. $V_{ac}(t)$ enhanced with a preamplifier was taken and analyzed using a fast-Fourier transform spectrum analyzer with time-resolutions that enable us to measure $V_{ac}(t)$ at f up to about 10 kHz [18, 35–38]. The film was directly immersed into the liquid ^{4}He and the magnetic field was applied perpendicular to the plane of the film.

3. Results and discussion

3.1. Ac current–voltage characteristics and estimation of the diameter of the pinning potential

Figure 1(a) shows $V_{ac,e}$ versus $I_{ac,e}$ of sinusoidal wave with $f = 80$ kHz (purple circles) and dc I–V characteristics (black circles) plotted on a log–log scale. The data points of dc $V(I)$ show a smooth downward curve, as typically observed in the vortex solid state. The dc depinning current I_d is determined to be about 0.24 mA, which corresponds to the threshold current at which the vortex motion ceases. The $I_{ac,e}$–$V_{ac,e}$ curve at 80 kHz is located above the dc I–V curve, reflecting the reduced pinning effect the moving vortices feel [24, 31]. The overall shape of the $I_{ac,e}$–$V_{ac,e}$ curve is similar to that of the dc I–V curve, however, a peculiar linear regime exists below a characteristic current $I_{ac,es} = 0.16$ mA and voltage $V_{ac,es} = 3.9\ \mu$V. Such a change in curvature is not observed for the dc I–V characteristics.

The inset of figure 1(a) schematically illustrates the pinning-potential well and oscillation of a vortex for three $V_{ac,e}$ regimes: $V_{ac,e} > V_{ac,es}$, $V_{ac,e} = V_{ac,es}$, and $V_{ac,e} < V_{ac,es}$ from top to bottom. In the regime of $I_{ac,e} < I_{ac,es}$ ($V_{ac,e} < V_{ac,es}$), the vortices are trapped in the pinning-potential well, where the mean displacement of the vortex oscillation around the initial position is smaller than the diameter d_p of the pinning potential, leading to a linear $I_{ac,e}$–$V_{ac,e}$ response. As $I_{ac,e}$ ($V_{ac,e}$) exceeds the characteristic value $I_{ac,es}$ ($V_{ac,es}$), the vortices are depinned from the pinning potential, where the mean displacement of the vortex oscillation is larger than d_p. This leads to a nonlinear $I_{ac,e}$–$V_{ac,e}$ response, similarly to the dc I–V case. Since the amplitude of the ac velocity v_{ac} is given by $v_{ac} = |V_{ac}|/Bl$, where l is the distance between the voltage contact, the mean diameter of the pinning potential is estimated to be $d_p \approx \sqrt{2}\, V_{ac,es}/\pi Blf + 2\xi \approx 10 + 18 = 28$ nm, where 2ξ ($\approx$18 nm) is the size of the vortex core estimated from the upper critical field.

In figure 1(b), all the $I_{ac,e}$–$V_{ac,e}$ curves taken at f ranging from 2 to 250 kHz are shown. The f-dependent characteristic current $I_{ac,es}$ and voltage $V_{ac,es}$ separating the linear and nonlinear regimes are observed for all f in the range $f = 2$–250 kHz. Note that features of the $I_{ac,e}$–$V_{ac,e}$ characteristics for different f, namely, the crossover from the linear relation at low $I_{ac,e}$ to the nonlinear one at high $I_{ac,e}$, as well as the upward shift of the

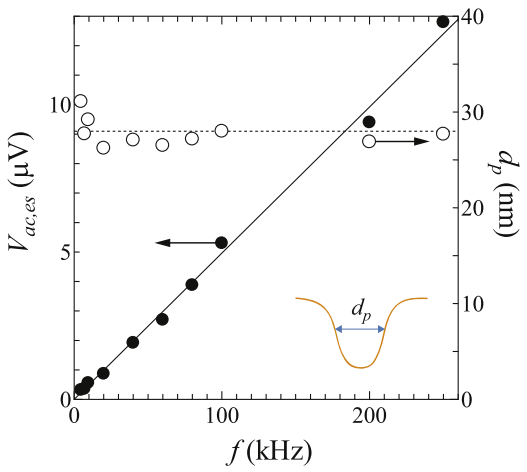

Figure 2. $V_{ac,es}$ (solid circles) and d_p (open circles) plotted against f. A full line represents the result of the linear fit and a horizontal dotted line is a guide for the eye. Inset: schematic diagram of the pinning-potential well with a diameter of d_p.

$V_{ac,e}(I_{ac,e})$ curves by increasing f, are qualitatively the same as what have been predicted numerically in figure 1(b) of [24]. In our data, with an increase in f, $V_{ac,es}$ increases significantly from around 0.27 to 13 μV, while $I_{ac,c}$ stays in a limited range 0.12–0.18 mA.

Shown in figure 2 with solid and open circles are f dependences of $V_{ac,es}$ obtained from the data in figure 1(b) and d_p calculated using the above-mentioned equation, respectively. All the data points of $V_{ac,es}$ fall onto nearly a single straight line expressed as $V_{ac,ec}/f = 5 \times 10^{-11}$ (V Hz^{-1}), which leads to a f-independent value of d_p. This fact strongly supports the validity of the picture mentioned above, and also implies that the measurements of $I_{ac,e}$–$V_{ac,e}$ curves for a limited number of f are sufficient to evaluate the average value of d_p. From the slope of the straight line, we immediately obtain $d_p = 28 \pm 2$ nm, which is comparable to the size of the vortex core (≈18 nm). This is consistent with the intuitive belief based on the structural studies of amorphous films and other indirect experimental evidence that the amorphous films contain point-like pinning centers [39–41]. However, we cannot state definitely whether the exact shape of the pinning centers is point-like or columnar-like, and to what extent they are uniform. Judging from the weak pinning strength in our a-Mo$_x$Ge$_{1-x}$ films, the columnar defects, such as created by heavy ions irradiation in oxide superconductors, are most likely absent. The well-determined value of $d_p = 28$ nm in our experiment suggests that the distribution of the pinning-potential wells may be fairly uniform. If our films contained a substantial number of pinning centers with d_p larger than 28 nm, the separation between the linear and nonlinear regimes in the $I_{ac,e}$–$V_{ac,e}$ characteristics would be more ambiguous.

3.2. Transient dynamics associated with dynamic ordering

Now, we focus on the transient behavior of vortices associated with dynamic ordering near the ac depinning threshold $I_{ac,d}(f)$ at a given frequency f. Hereafter, the applied ac current $I_{ac}(t)$ is of square waveform, similarly to that used in previous work on the reversible to irreversible flow transition [18, 36, 38, 42]. First, we estimate the depinning current $I_{ac,d}(f)$ in the steady state from the $|I_{ac}|$–$|V_{ac}|$ characteristics, where $|I_{ac}|$ and $|V_{ac}|$ represent the amplitude of the applied ac current and that of the induced voltage, respectively. $I_{ac,d}(f)$ is defined as a current $|I_{ac}|$ at which $|V_{ac}|$ in the nonlinear regime, namely, the amplitude of the velocity of vortices that are oscillating around the pinning centers in mean distances larger than the pinning diameter d_p is smoothly extrapolated to zero with a decrease in $|I_{ac}|$. Specifically, we fit the data in the nonlinear regime near the depinning threshold to an empirical formula $|V_{ac}| \propto (|I_{ac}| - I_{ac,d})^{\beta}$ with $\beta > 1$. In figure 3(a), we plot $|V_{ac}|$ against $|I_{ac}|$ at various f ranging from 0.06 to 250 kHz with colored symbols and, for comparison, dc I–V characteristics with black circles. The best fit for the ac and dc data are achieved using $\beta = 2.2 \pm 0.2$ and 2.4 ± 0.2, respectively. The results of the fit for selected f including dc ($f = 0$) are shown with full lines in figure 3(a), and those for the ac data at $f = 0.06$–9.5 kHz and dc data are indicated with red and black lines in 3(b), respectively. For dc data, $I_{ac,d}$ is replaced by the depinning current I_d determined from the dc I–V characteristics. It is found that when $|V_{ac}(f)|$ is plotted against $|I_{ac}(f)| - I_{ac,d}(f)$ on a log–log scale, as shown in figure 3(b), all the data points in the frequency range $f = 0.06$–9.5 kHz fall onto nearly a single line expressed as $\log|V_{ac}| = \beta \log(|I_{ac}| - I_{ac,d}) + b$, where β and b are constants independent of f. In the inset of figure 3(a), the depinning current $I_{ac,d}$ thus obtained is plotted against f. $|I_{ac,d}(f)|$ shows a trend to decrease with increasing f, which reflects the reduced pinning effect at higher f.

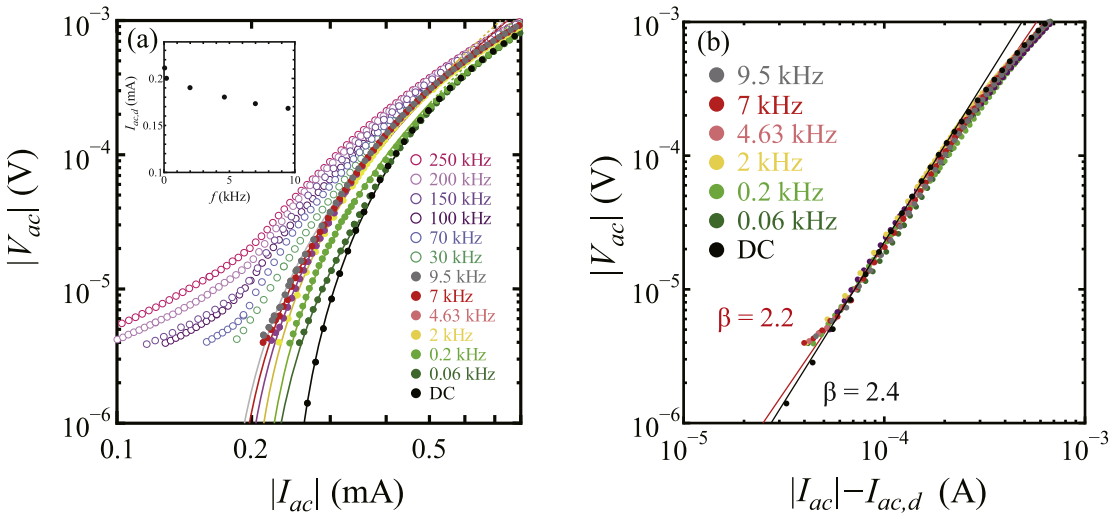

Figure 3. (a) $|V_{ac}|$ versus $|I_{ac}|$ for square wave at various f listed in the figure. Black circles represent the dc $I-V$ characteristics. Full lines indicate the results of the fit. Inset: f dependence of $I_{ac,d}$. (b) $|V_{ac}|$ plotted against $|I_{ac}| - I_{ac,d}$ on a log–log scale. Red and black lines represent the results of the fit of the ac data at $f = 0.06$–9.5 kHz and dc data, respectively.

Next, we present the data of the time-dependent voltage $V_{ac}(t)$ generated in response to the ac current $I_{ac}(t)$ of square waveform. In this transient measurement, the maximum frequency f of I_{ac} was limited to 10 kHz due to the time resolution of our fast-Fourier transform spectrum analyzer. We know from our earlier work that for the ac driven vortices, the dynamic ordering process for a disordered initial vortex configuration is more easily detected than the dynamic disordering process for an ordered initial configuration [18, 36, 38]. Therefore, in this work we study the transient motion of vortices associated with dynamic ordering using the following experimental procedure: first, the vortex system is driven by a dc current I that generates $V = 10\ \mu$V, which gives rise to a disordered plastic-flow state in the steady state. Then, its configuration is frozen by abruptly switching off the current I. Thus prepared vortex lattices are highly disordered, containing a large number of dislocations, and strongly pinned by random pinning centers [36, 42]. Subsequently, $I_{ac}(t)$ is applied at $t = 0$ and $V_{ac}(t)$ is measured until the final steady state is reached. Since the voltage is proportional to the mean velocity of vortices, a transient motion of vortices can be detected by measuring $V_{ac}(t)$. We repeat this measurement of $V_{ac}(t)$ by changing the amplitude of $I_{ac}(t)$ with small current steps. Note that we are not able to examine the transient behavior of the ac depinning transition in the pinned phase ($|I_{ac}| < I_{ac,d}$), where $V^{\infty} = 0$.

In figures 4(a)–(c), we show the selected data of $V_{ac}(t)$ generated by 2 kHz $I_{ac}(t)$ with amplitudes of 0.32, 0.37, and 0.66 mA, which yield $V^{\infty} = 40,\ 90$, and 600 μV, respectively. The location of V^{∞} is indicated by horizontal dashed lines. Regardless of the value of V^{∞}, the amplitude of the voltage at $t = 0$, $|V_{ac}(t = 0)|(\equiv V_0)$, is smaller than V^{∞} and $|V_{ac}(t)|$ shows a gradual increase to a saturation value of V^{∞}. This behavior is explained as follows: the initial vortex configuration is highly disordered deformed lattices, where many vortices are strongly pinned by random pinning centers. When the ac drive $|I_{ac}|$ larger than $I_{ac,d}$ is applied, some vortices escape from the pinning potential and take part in the flow states, which in turn facilitates further depinning. Therefore, the mean velocity of vortices, $|V_{ac}(t)|$, increases until the final steady state is reached. For larger V^{∞}, the transient behavior of $|V_{ac}(t)|$ is less pronounced. This is because for the larger ac driving force $|I_{ac}|$ giving rise to larger V^{∞}, both the depinning and dynamic ordering (or healing) processes are promoted, resulting in faster relaxation.

3.3. Critical behavior near the ac depinning transition

To explore the critical behavior of the depinning transition by the ac drive, we extract the characteristic time τ for the system to reach the steady state by fitting the amplitude of the ac voltage $|V_{ac}(t)|$ to the theoretical relaxation function [2, 43],

$$|V_{ac}(t)| = V^{\infty} - (V^{\infty} - V^{0})\exp(-t/\tau)/t^{\alpha}. \quad (1)$$

Here, we fix the value of α to be zero, because theoretically α is relevant only very close to the transition ($\tau \to \infty$), while in our experiment τ/t is relatively small [18]. The results of the fit are shown with dotted lines in figures 4(a)–(c). The values of τ obtained from the fit are shown in the main panel of figure 5(a), where τ's at $f = 2$ kHz (yellow circles) and at other frequencies in the range $f = 0.06$–7 kHz are plotted as a function of $|I_{ac}|$. The divergence of τ is clearly visible at the f-dependent characteristic current, which is nearly equal to the depinning current $I_{ac,d}$ obtained above from the steady-state $|I_{ac}|$–$|V_{ac}|$ measurements (see the inset of

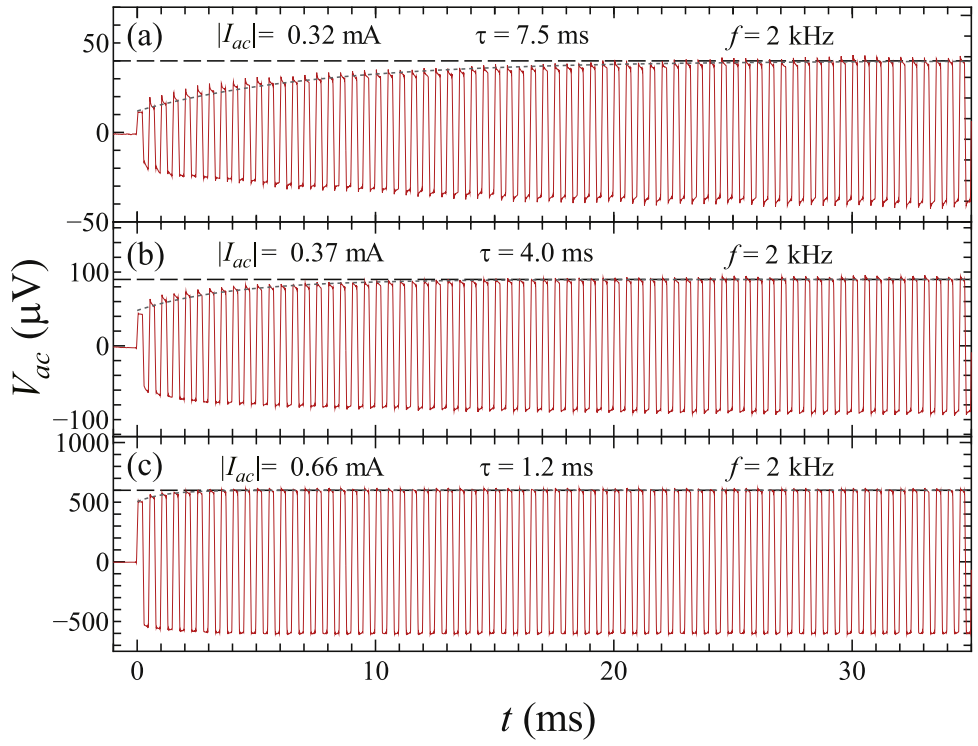

Figure 4. Selected data of $V_{ac}(t)$ generated by 2 kHz $I_{ac}(t)$ with amplitudes of (a) 0.32, (b) 0.37, and (c) 0.66 mA yielding $V^{\infty} = 40$, 90, and 600 μV, respectively. Dotted lines are results of the fit and horizontal dashed lines indicate the location of V^{∞}.

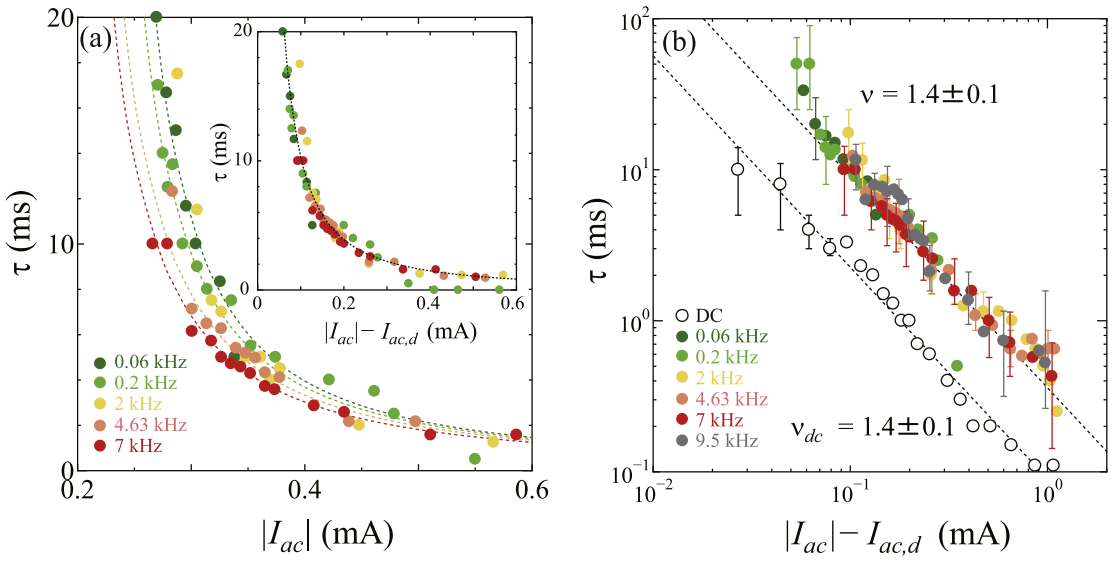

Figure 5. (a) τ plotted against $|I_{ac}|$ for selected frequencies f, which are listed in the figure. The dotted lines are the results of the power-law fit. Inset: τ versus $|I_{ac}| - I_{ac,d}$, where the symbols correspond to those in the main panel. A dotted line represents the result of the power-law fit. (b) τ versus $|I_{ac}| - I_{ac,d}$ (colored symbols) on a log–log scale. The gray circles represent the data at 9.5 kHz and other symbols correspond to those in (a). τ's obtained from the dc data are also shown with open black circles. Ac and dc data are measured from the disordered and ordered initial configurations, respectively. The dotted straight lines indicate the results of the power-law fit, both of which give the same exponent of 1.4.

figure 3(a)). This result strongly suggests that the nonequilibrium depinning transition occurs not only for the dc drive but also for the ac drive, and that $I_{ac,d}$ obtained from $|I_{ac}|$–$|V_{ac}|$ characteristics indeed corresponds to the ac depinning transition. Large errors of τ are present for smaller τ in the large $|I_{ac}|$ region, which are more remarkable at lower f. This is because with a decrease in f, the pulse width of $V_{ac}(t)$ increases as $\propto 1/f$, and when the width approaches $\tau \sim 1$ ms, it becomes difficult to precisely determine τ in ms from the fit using equation (1). Interestingly, when the same data of τ as shown in the main panel of figure 5(a) are plotted against

$|I_{ac}| - I_{ac,d}$, all the data collapse on a single curve, as shown in the inset of figure 5(a). Here, the dotted lines represent the fits of the data to a power-law function $\tau \propto (|I_{ac}| - I_{ac,d})^{-\nu}$ with $\nu = 1.4 \pm 0.1$.

In figure 5(b), all the data shown in the inset of figure 5(a), including the data at 9.5 kHz (gray circles), are plotted on a log–log scale, where the colored symbols correspond to those in the inset of figure 5(a). A dotted (upper) straight line represents the result of the power-law fit, and the slope gives $\nu = 1.4 \pm 0.1$. For comparison, the result of the dc depinning transition, τ versus $I - I_d$, is also shown with black open circles, where we prepared an ordered initial vortex configuration and a transient behavior associated with dynamic disordering was measured. The reason why we used the ordered initial configuration for the dc depinning experiment is that it is more difficult to obtain accurate values of τ in the dynamic ordering process. This is in contrast to the case of the ac depinning experiment, where the transient behavior associated with the dynamic ordering is clearly observed. The difference in the initial vortex configuration may account for the difference between the fitted lines of τ for the ac and dc depinning experiments. If we could conduct a dc depinning experiment that exhibits dynamic ordering using a highly disordered initial vortex configuration, or an ac depinning experiment that exhibits dynamic disordering using a highly ordered initial vortex configuration, the merging of the ac and dc data might be expected in figure 5(b). The argument here also implies that the values of the relaxation time τ at a given driving force should depend on the initial conditions, although they may be of the same order of magnitude.

In our independent study using the vortex system of a-Mo_xGe_{1-x} films, it has become clear that the dynamic ordering (or random organization) by the ac drive, which was detected from the $V_{ac}(t)$ data, such as shown in figures 4(a)–(c), is responsible for the reversible–irreversible transition [18, 36, 38, 42]. Note, however, that the experimental parameter driving the reversible–irreversible transition is a frequency f, that is, a displacement amplitude of vortices per cycle at a *fixed* mean velocity [18, 36, 38, 42], whereas the parameter driving the ac depinning transition is the amplitude of the ac driving force or, equivalently, the mean velocity in the steady state. Furthermore, the critical points of the two transitions are different: for the reversible–irreversible transition, the critical point of the transition corresponds to the (non-fluctuating) moving state where the vortices oscillate with a relatively small amplitude but much larger than d_p and, hence, $|V_{ac}|(\equiv V^{\infty})$ is nonzero in the steady state [18, 36, 38, 42]. In contrast, the critical point of the ac depinning transition corresponds to the quiescent state in the limit $|V_{ac}(|I_{ac}| \to I_{ac,d} + 0)| \to 0$, where all vortex motion ceases. It is also noted that for the study of the reversible–irreversible transition the relaxation time τ is expressed as a number of cycles instead of time in seconds. Thus, it may be interesting to express τ for the ac depinning transition as a number of cycles, which may lead to a more profound view on the dynamic ordering by ac drive, associated with the reversible–irreversible transition and depinning transition. We leave this issue for future work, and here we simply show in figure 5(b) that τ's (in seconds) associated with the ac and dc depinning transitions are of the same order.

An important finding in this work is that, while the threshold $I_{ac,d}$ of the ac depinning transition is dependent on f, the critical behavior of τ near the transition is independent of f, which is characterized by the critical exponent $\nu = 1.4 \pm 0.1$ and this value is identical to the one ($\nu_{dc} = 1.4 \pm 0.1$) for the dc depinning transition [18, 29]. Note that $\nu = 1.4$ is also close to the exponent ($\nu = 1.3$) for the reversible–irreversible flow transition found in the two-dimensional vortex system [18, 38, 42], which was originally found in colloidal suspensions for three-dimensions ($\nu = 1.1$) [43–45], and close to $\nu = 1.2$ for the absorbing state transition [46, 47] reported in the liquid-crystal system [48, 49]. The results obtained in this work demonstrate that the nonequilibrium depinning transition occurs not only for the dc drive but also for the ac drive, which can further support the theoretical prediction that the plastic depinning transition may fall into the same universality class as the reversible–irreversible transition and the absorbing state transition [2].

4. Conclusions

We study the general phenomenon of plastic depinning, focusing on whether the critical behavior of vortex dynamics near the dc depinning transition, which has been found experimentally [18, 29] as well as numerically [2], is also observed for the ac drive. For the study of the ac depinning transition, however, the influence of the nonzero diameter $d_p(>0)$ of the pinning-potential well must be taken into account. From the $I_{ac,e}$–$V_{ac,e}$ characteristics for different f, where $V_{ac,e}$ and $I_{ac,e}$ are the effective voltage and current of sinusoidal waveform, respectively, we clearly identify the f-dependent characteristic current $I_{ac,es}$ and voltage $V_{ac,es}$ separating the linear response regime ($V_{ac,e} < V_{ac,es}$) where vortices oscillate inside the pinning-potential well from the nonlinear regime ($V_{ac,e} > V_{ac,es}$) where depinning from the pinning potential occurs. These features are qualitatively the same as those reported numerically [24]. Based on the $V_{ac,es}$–f relation obtained here, the mean diameter d_p is estimated to be about 28 nm, which is nearly independent of f. We propose that the method presented here is a very convenient way for estimating d_p, which is important for the practical applications of superconductivity.

We also measure the transient $V_{ac}(t)$ for the disordered initial vortex configuration in response to the ac drive $I_{ac}(t)$ of square waveform. $|V_{ac}(t)|$ exhibits a gradual increase towards the steady-state voltage, indicative of dynamic ordering. The relaxation time τ to reach the steady state increases with a decrease in $|I_{ac}|$, and shows a power-law divergence at the f-dependent threshold, which is equal to the depinning current $I_{ac,d}(f)$ determined from the $|I_{ac}|$–$|V_{ac}|$ characteristics in the nonlinear regime. When τ is plotted against $|I_{ac}(f)| - I_{ac,d}(f)$, all the data at different f fall onto nearly a single line expressed as $\tau \propto (|I_{ac}| - I_{ac,d})^{-\nu}$ with a critical exponent $\nu = 1.4$, which almost coincides with the value for the dc depinning transition [18, 29]. These results indicate that the critical behavior of the depinning transition is observed not only for the dc-driven vortex system but also for the ac-driven one, further demonstrating the universality of the nonequilibrium depinning transition.

Acknowledgments

This work was supported by a Grant-in-Aid for Scientific Research from the Ministry of Education, Culture, Sports, Science, and Technology of Japan. YK acknowledges the financial support from the Global Center of Excellence Program by MEXT, Japan through the 'Nanoscience and Quantum Physics' Project of the Tokyo Institute of Technology.

References

[1] Olson C J, Reichhardt C and Nori F 1998 *Phys. Rev. Lett.* **81** 3757
[2] Reichhardt C and Olson Reichhardt C J 2009 *Phys. Rev. Lett.* **103** 168301
[3] Oda M and Ido M 1984 *Bussei Kenkyu* **41** 161
[4] Fisher D S 1985 *Phys. Rev.* B **31** 1396
[5] Wang Z Z and Ong N P 1987 *Phys. Rev. Lett.* **58** 2375
[6] Henderson W, Andrei E Y and Higgins M J 1998 *Phys. Rev. Lett.* **81** 2352
[7] Marchetti M C and Dahmen K A 2002 *Phys. Rev.* B **66** 214201
[8] Dröse T, Besseling R, Kes P and Smith C M 2003 *Phys. Rev.* B **67** 064508
[9] Charalambous D *et al* 2006 *Phys. Rev.* B **73** 104514
[10] Maeda A and Nakamura D 2007 *J. Phys.: Conf. Ser.* **89** 012020
[11] Luo M B and Hu X 2007 *Phys. Rev. Lett.* **98** 267002
[12] Pertsinidis A and Ling X S 2008 *Phys. Rev. Lett.* **100** 028303
[13] Moretti P and Miguel M C 2009 *Phys. Rev.* B **80** 224513
[14] Mangan N, Reichhardt C and Olson Reichhardt C J 2008 *Phys. Rev. Lett.* **100** 187002
[15] Mohan S, Sinha J, Banerjee S S, Sood A K, Ramakrishnan S and Grover A K 2009 *Phys. Rev. Lett.* **103** 167001
[16] Fily Y, Olive E, Scala N D and Soret J C 2010 *Phys. Rev.* B **82** 134519
[17] Zhang W, Zhou W and Luo M 2010 *Phys. Lett.* A **374** 3666
[18] Okuma S, Tsugawa Y and Motohashi A 2011 *Phys. Rev.* B **83** 012503
[19] Misko V R and Nori F 2012 *Phys. Rev.* B **85** 184506
[20] Thomann A U, Geshkenbein V B and Blatter G 2012 *Phys. Rev. Lett.* **108** 217001
[21] Silhanek A V *et al* 2012 *New J. Phys.* **14** 053006
[22] Pi U H, Cho Y J, Bae J Y, Lee S C, Seo S, Kim W, Moon J H, Lee K J and Lee H W 2011 *Phys. Rev.* B **84** 024426
[23] Tamura K, Ozawa T, Bando Y, Kawamoto T and Mori T 2010 *J. Appl. Phys.* **107** 103716
[24] Pérez Daroca D, Lozano G S, Pasquini G and Bekeris V 2010 *Phys. Rev.* B **81** 184520
[25] Pérez Daroca D, Pasquini G, Lozano G S and Bekeris V 2011 *Phys. Rev.* B **84** 012508
[26] Ganguli S C, Singh H, Roy I, Bagwe V, Bala D, Thamizhavel A and Raychaudhuri P 2016 *Phys. Rev.* B **93** 144503
[27] Reichhardt C and Olson Reichhardt C J 2017 *Rep. Prog. Phys.* **80** 026501
[28] Shaw G, Mandal P, Banerjee S S, Niazi A, Rastogi A K, Sood A K, Ramakrishnan S and Grover A K 2012 *Phys. Rev.* B **85** 174517
[29] Okuma S and Motohashi A 2012 *New J. Phys.* **14** 123021
[30] Miguel M C and Zapperi S 2003 *Nat. Mater.* **2** 477
[31] Valenzuela S O 2002 *Phys. Rev. Lett.* **88** 247003
[32] Pautrat A, Goupil C, Simon C, Charalambous D, Forgan E M, Lazard G, Mathieu P and Brûlet A 2003 *Phys. Rev. Lett.* **90** 087002
[33] Nojima T, Takahashi K, Chotoku M, Ochiai A, Aoki H, Lee H G and Lee S I 2009 *J. Phys.: Conf. Ser.* **150** 052189
[34] Okuma S, Motohashi A and Kawamura Y 2013 *Phys. Lett.* A **377** 2990
[35] Okuma S, Inoue J and Kokubo N 2007 *Phys. Rev.* B **76** 172503
[36] Okuma S, Kawamura Y and Tsugawa Y 2012 *J. Phys. Soc. Japan* **81** 114718
[37] Okuma S, Kashiro K, Suzuki Y and Kokubo N 2008 *Phys. Rev.* B **77** 212505
[38] Nitta R, Kawamura Y, Kaneko S and Okuma S 2015 *Phys. Proc.* **65** 105
[39] Kokubo N, Okayasu S, Kanda A and Shinozaki B 2010 *Phys. Rev.* B **82** 014501
[40] Kokubo N, Nishizaki T, Shinozaki B and Kes P H 2010 *Physica* C **470** 43
[41] Okuma S, Shimamoto D and Kokubo N 2012 *Phys. Rev.* B **85** 064508
[42] Dobroka M, Kawamura Y, Ienaga K, Kaneko S and Okuma S 2017 *New J. Phys.* **19** 053023
[43] Corté L, Chaikin P M, Gollub J P and Pine D J 2008 *Nat. Phys.* **4** 420
[44] Pine D J, Gollub J P, Brady J F and Leshansky A M 2005 *Nature* **438** 997
[45] Gollub J and Pine D 2006 *Phys. Today* **59** 8
[46] Hinrichsen H 2000 *Adv. Phys.* **49** 815
[47] Dickman R 2002 *Physica* A **306** 90
[48] Takeuchi K A, Kuroda M, Chaté H and Sano M 2007 *Phys. Rev. Lett.* **99** 234503
[49] Takeuchi K A 2014 *J. Stat. Mech.* P01006